Journal of Power Sources 412 (2019) 272–281

Contents lists available at ScienceDirect

Journal of Power Sources

journal homepage: www.elsevier.com/locate/jpowsour

Mechanical behavior and Weibull statistics based failure analysis of vanadium flow battery stacks

Jing Xiong[a,b], Shaoliang Wang[a], Xiangrong Li[a,**], Zhigang Yang[a], Jianguo Zhang[a], Chuanwei Yan[a], Ao Tang[a,*]

[a] Institute of Metal Research, Chinese Academy of Sciences, Shenyang, China
[b] School of Materials Science and Engineering, University of Science and Technology of China, Shenyang, China

HIGHLIGHTS

- The Weibull parameters of key stack components are determined from tensile tests.
- Mechanical behaviors of the stack components are analyzed by finite element method.
- The failure probabilities of the key components and the stack are calculated.
- Introducing a thick plate can significantly improve the reliability of the stack.

GRAPHICAL ABSTRACT

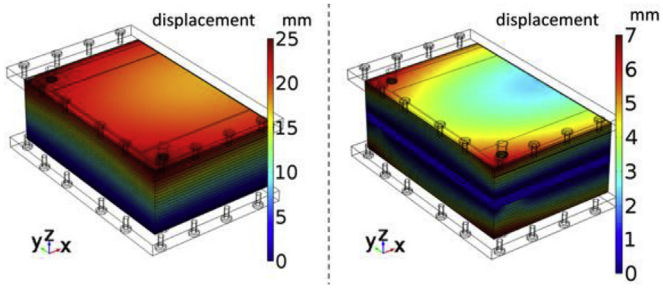

ARTICLE INFO

Keywords:
Vanadium redox flow battery
Mechanical behavior
Weibull statistics
Failure probability
Finite element analysis

ABSTRACT

Stack reliability is of great importance in commercialization of vanadium redox flow battery (VFB) since practical VFB stacks are prone to undergo material failure and electrolyte leakage caused by unreliable stack design and improper assembling conditions. A comprehensive evaluation of mechanical behavior and analysis of stack failure is thus highly valued for material fabrication, stack design and assembly. In this study, mechanical behavior and Weibull statistics based failure analysis of the VFB stacks are investigated. The Weibull parameters of two key components are firstly determined from tensile strength tests, which, in combination with finite element analysis of the stack mechanical behavior, are subsequently used to calculate the stack failure probability at specified clamping forces for two different stack designs that both contains 20 individual cells. The results demonstrate that the stack failure probability can be significantly reduced by properly decreasing the clamping forces for both designs, while adding a thick plate to the middle of the stack can effectively lower the probability of failure thus offering a superior stack mechanical performance and a prolonged stack life cycle. Such an approach to analyze stack failure can be readily accessed by flow battery engineers for design and assembly of commercial VFB stacks.

1. Introduction

Large-scale cost effective energy storage has become one of the most pressing issues in the world today due to the rapid development of renewable, yet unstable, forms of energy. Among the currently available energy storage technologies, electrochemical energy storage

* Corresponding author.
** Corresponding author.
E-mail addresses: xrli@imr.ac.cn (X. Li), a.tang@imr.ac.cn (A. Tang).

https://doi.org/10.1016/j.jpowsour.2018.11.060
Received 10 April 2018; Received in revised form 26 September 2018; Accepted 17 November 2018
Available online 29 November 2018
0378-7753/

system offers the best combination of efficiency, cost and lifetime, with flow batteries leading the way in this aspect [1]. Of all the flow batteries, the all-vanadium redox flow battery (VFB) has to date exhibited the greatest potential for large-scale electrical energy storage applications with the merit of the use of same element in both half-cells that fully prevents the cross-contamination and enables a theoretically indefinite electrolyte life [2,3]. As with all the other flow batteries, the VFB also offers a great flexibility in designing the power output and capacity independently, so a commercial VFB stack is seen to be fabricated by dozens or even hundreds of individual unit flow cells so as to meet the power demands for the specified applications [4,5].

Generally, a good VFB stack should have excellent cycling performance in terms of energy efficiency while exhibiting great mechanical performance as well. For commercial stacks, in particular, more focuses should be on mechanical design and assembly of the stack, as reliable stacks can significantly reduce the cost associated with material replacement and stack maintenance and thereby make more profits in the entire life cycle. To date, the most widely used stack assembling method adopted by flow battery manufacturers relies on clamping all individual cells within two thick end-plates in conjunction with dozens of spring bolts fixed at the edges of end-plates [6,7]. Despite forming a leak-proof assembly, it is still a big challenge to avoid stack leakage arising from inappropriate assembling force in terms of both location and magnitude, as commercial VFB stacks are commonly made by dozens of cells connected in series with each cell comprised of multiple components with fairly different material properties and structure designs [8] (e.g. perfluorinated membrane [9,10], non-corrosive flow frame with embedded flow channels [11,12], conducting composite bipolar plate [13,14], porous carbon or graphite electrode [15,16] and non-corrosive sealing gasket). Evidence in practice has demonstrated that improper assembling design can yield notable non-uniform stress distribution on adjacent stack components inducing undesirable leakage, and even result in material failure and crack exacerbating electrolyte leakage when applied stress exceeds the strength of the material according to yield criterion. In contrast to conventional clamping-based assembly method, some alternative techniques (e.g. laser welding) have also been developed to avoid electrolyte leaks, but they still face certain limitations when applied to assemble large commercial stacks (e.g. high manufacture cost and restricted welding conditions). In order to further optimize the stack sealing design for the conventional assembly method, mathematical modeling and simulation method is an effective tool to evaluate the stress distribution on stack components under a given assembling force, e.g. finite element analysis which has proved to be a viable solution to assess mechanical behaviors of fuel cell stacks [17,18]. Apart from that, our recent study has also, for the first time, utilized finite element method to successfully develop a three-dimensional mechanical model and analyze stresses in flow battery stacks under specified stack design and assembling conditions [19].

Although mechanical behavior of VFB stack material and component can be analyzed by finite element method, flow battery engineers still urgently require a way to associate mechanical simulation results with stack reliability evaluation, ultimately supervising the stack design and assembly from the viewpoint of engineering and fabrication. Our previous study [19] analyzed the stress distribution on the key components of the VFB stack under different clamping forces. The results have demonstrated that larger stresses are mainly received on the regions where the thin gaskets are located. Owe to its ductile property, the membrane can generally withstand a large stress and is less likely to fracture. Engineering experience yet reveals a high failure or fracture probability in bipolar plate and flow frame where electrolyte leakages tend to occur, which can be attributed to their brittle properties. For such a brittle material, its material strength normally obeys a statistic distribution, i.e. Weibull distribution. Thus, the Weibull statistic method can be employed to evaluate the failure probabilities of bipolar plate and flow frame under an applied stress, based on which the failure probability of VFB stack can be subsequently determined. Examples in literature have already demonstrated the feasibility of Weibull statistic method in evaluating the mechanical behavior of stack for fuel cell applications. Some researchers [19–23] simulated thermal stresses of the solid oxide fuel cells by using the finite element tools and subsequently compute the failure probability of the cells based on the stresses with Weibull analysis, while Clague et al. [24] predicted both time-independent and time-dependent probability of failure of the ceramic layers of a solid oxide fuel cell by using the weakest link theory and the Weibull method. Greco et al. [25] investigated the significance of the relaxation of the stresses by creep in the cell components and its influence on the probability of cell survival, followed by the influence of cell size on the failure probability. For VFB stacks, therefore, the Weibull statistics analysis in conjunction with mechanical simulation results can offer a viable and practical solution for engineers to evaluate the failure probability of stack and guide the stack design and assembly from an engineering point of view.

In this paper, mechanical behavior and Weibull statistics based failure analysis of the VFB stacks are for the first time investigated. This study firstly introduces the fabrication of bipolar plate and flow frame and describes the measurement of their tensile strengths, followed by proposing the calculation of failure probabilities of bipolar plate and flow frame based on Weibull statistics analysis. To evaluate the failure probability of the stack and optimize stack design, finite element modeling and analysis in association with Weibull statistics method are subsequently performed for a 20-cell stack with two different stack designs. Finally, the results demonstrate that by adding a thick plate to the middle of the stack, not only the stack failure probability can be significantly reduced but a superior sealing performance and a reduction in contact resistance can be also achieved, thereby effectively prolonging the stack life cycle. Such a failure analysis approach can be readily applied to the design and assembly of commercial VFB stacks that ensures reliable mechanical and sealing performance in long-term operation.

2. Experimental

As described above, the flow frame and bipolar plate are shown to be the two components in a practical VFB stack which are most likely to suffer from mechanical damage since they are brittle. Therefore, the effects of material properties of the flow frame and the bipolar plate on failure probability of the stack are analyzed in detail in this section. The fabrication processes are firstly described, followed by the measurements of their mechanical properties in tensile tests. Subsequently, Weibull statistics and failure probability are proposed which, together with finite element analysis, are used to investigate the assembling conditions and mechanical performance of the practical VFB stacks.

2.1. Fabrications of bipolar plate and flow frame

The fabrication process of the composite bipolar plates, made of a thermoplastic resin plate, carbon materials and conductive fillers, comprises two steps. First of all, the low-conductive plastic plate was conducted by filling the conductive fillers into the thermoplastic resin-latticed plate through hot-pressing at 200 °C under a pressure of 15 MPa for ca. 100 min. The obtained low-conductive plastic was subsequently coated with carbon materials, i.e. the mixture of graphite and carbon fiber powder, on both sides by hot-pressing in the same conditions as described above. Furthermore, the flow frames were prepared with polyvinyl chloride processing in a screw injection molding machine at 180 °C. The injection pressure and holding pressure were 120 MPa and 70 Mpa respectively and the rotation speed of the screw is ca. 30 r min^{-1}. More detailed information regarding fabrications of bipolar plate and flow frame and stress-strain curves can be found in Supplementary Material.

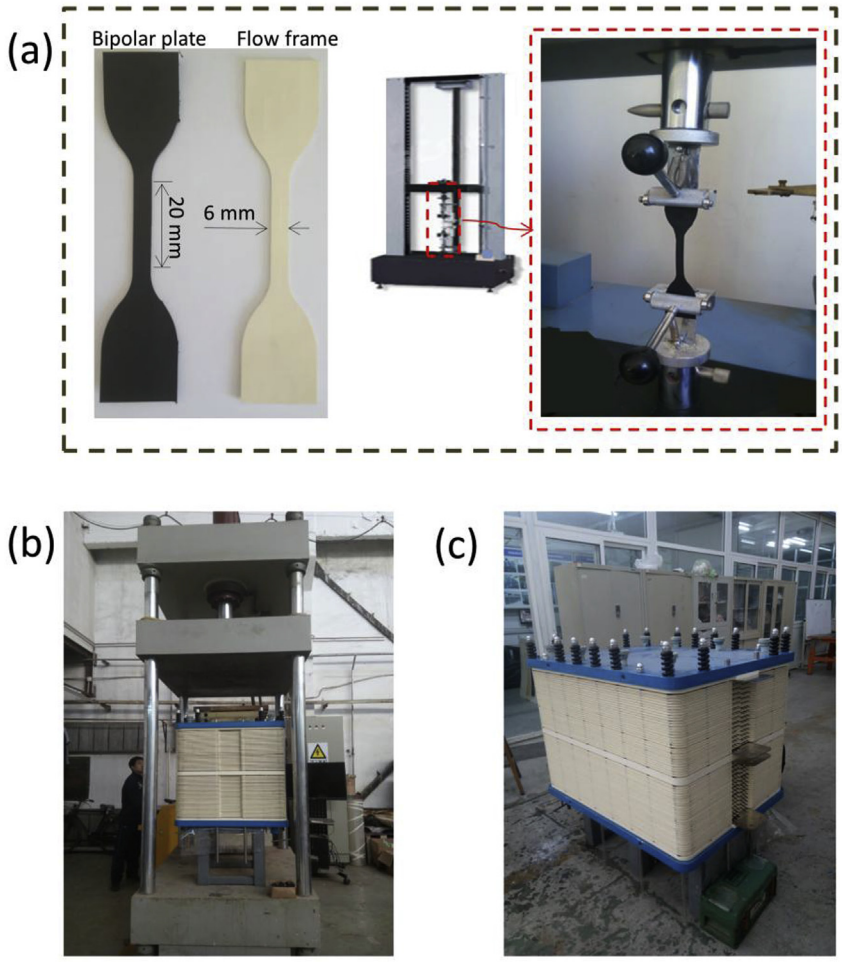

Fig. 1. Illustrations of tensile test and stack assembly. (a) Tensile tests of the flow frame and the bipolar plate; (b) Stack assembly process; (c) An assembled stack.

2.2. Mechanical properties and tensile tests

All the key components of the VFB apart from the electrodes bear both compression and tension. Among them, the bipolar plate and the flow plate in practice are prone to crack near the edges under a tensile stress. This is because the dislocation of the sealing gaskets may generate a tensile stress that pulls the bipolar plate and the flow frame outward. In order to perform Weibull statistical analysis and explore the failure of components, the tensile tests for the bipolar plates and flow frame were carried out. The tensile strengths of the flow frame and the bipolar plate prepared by above fabrication process were measured by tensile tests with dumbbell specimens. The samples are cut by milling with a thickness of 1 mm, a width of 6 mm and a gauge length of 20 mm as shown in Fig. 1(a). The tests were performed at room temperature on a mechanical tensile test machine. When the tensile strength σ is obtained, Weibull parameters, i.e. Weibull modulus m and scale parameter σ_0, for both flow frame and bipolar plate can be calculated on the basis of Weibull statistic theory.

2.3. Weibull statistics

Weibull statistic theory was developed by Weibull using the idea that, when one link in a chain fails, the whole chain fails [26]. The theory can be used to compute the failure probability of a structure, which is assumed as a chain with n links and each link with different failure strength. According to this theory, the cumulative failure probability P of a material subjected to a stress σ is given by Ref. [27].

$$P = 1 - \exp\left(-\left(\frac{\sigma - \sigma_u}{\sigma_0}\right)^m\right) \quad (1)$$

where m is the Weibull modulus, σ_u is the threshold stress below which no failures can occur, σ_0 is the scale parameter with the same dimension as σ. In general, the threshold σ_u is supposed to be zero, and hence the Weibull distribution function can be simplified as [28–30].

$$P = 1 - \exp\left(-\left(\frac{\sigma}{\sigma_0}\right)^m\right) \quad (2)$$

For Weibull analysis of tensile strength data, the samples are ordered by ascending strength in rank method, and the failure probability P of each sample is then approximated by Ref. [31].

$$P_i = \frac{i}{N+1} \quad (3)$$

where i is for the ith sample and N is the total number of samples tested. By rearranging Eq. (2), a linear equation is obtained with two dependent variables, $\ln(\ln(1/(1-P_i))$ and $\ln(\sigma_i)$

$$\ln\left(\ln\left(\frac{1}{1-P_i}\right)\right) = m\cdot\ln\sigma_i - m\cdot\ln\sigma_0 \quad (4)$$

where σ_i ($i = 1, 2, \ldots\ldots, N$) is the measured strength data for each sample. When $\ln(\ln(1/(1-P_i))$ is plotted against $\ln(\sigma_i)$ for the measured data, it is then possible to fit a straight line through the points. Finally, Weibull modulus m and scale parameter σ_0 can be obtained by the slope and the intercept of the fitted line.

2.4. Failure probability

In order to calculate the failure probabilities of each component and the whole stack more accurately, the integral form of failure probability is adopted. Probability of failure of the ith link P_i, with a volume V_i, subjected to a stress σ, can be expressed as [32,33].

$$P_i = 1 - \exp\left[-\iiint_{V_i}\left(\frac{\sigma - \sigma_u}{\sigma_0}\right)^m dV_i\right] \quad (5)$$

As mentioned previously, the threshold σ_u is supposed to be zero. Thus, Eq. (5) can also be written as

$$P_i = 1 - R_i = 1 - \exp\left[-\iiint_{V_i}\left(\frac{\sigma}{\sigma_0}\right)^m dV_i\right] \quad (6)$$

where $exp\left[-\iiint_{V_i}\left(\frac{\sigma}{\sigma_0}\right)^m dV_i\right]$ is the reliability (survival probability) of the ith link, R_i [20].

For a given applied stress, failure probability and reliability of assembled structure can be calculated according to Eqs. (7) and (8) [27,34].

$$R_{\text{structure}} = \prod_{i=1}^{N} R_i = \prod_{i=1}^{N} (1 - P_i) \quad (7)$$

$$P_{\text{structure}} = 1 - R_{\text{structure}} = 1 - \prod_{i=1}^{N} (1 - P_i) \quad (8)$$

where N is the number of components in the assembled structure.

2.5. Finite element analysis

In order to evaluate the failure probability of the stack and optimize the stack design, finite element modeling and analysis are performed for two different stack designs, one containing 20 cells and the other that also has 20 cells but with an additional thick plate placed in the middle (refer to as 20-cell-TPM stack), as demonstrated in Fig. 2(a) and (b) respectively. Both stack designs are introduced into COMSOL Multiphysics 5.1 for finite element analysis, and the finite element meshing of the 20-cell stack can be seen in Fig. 2(c). It is noted that the stack is shown in halved geometry for a reduction of computation time, as our previous study has demonstrated that the stress distribution in a VFB stack is symmetric [19]. The stack geometry and dimension are chosen from a practical 32 kW stack as displayed in Fig. 1(b) and (c), which along with the material properties are listed in Table 1 and Table 2. In an effort to mesh the model for a minimized computational time while without compromising the accuracy of analysis, the mesh independence analysis was also performed. Table 3 presents the effect of element number on the maximum principal stress of the flow frame in the 20-cell stack at a clamping force of 400 kN, where the stress is seen to vary slightly as the element number increases from 676,470 to 710,683. Therefore, the model meshed with an element number of 676,470 was chosen for the simulation in this study. Detailed information regarding governing equations and boundary conditions can be found in Supplementary Material.

Table 1
Geometric parameters of the stack components.

	Length (mm) x – axial	Height (mm) y – axial	Thickness (mm) z - axial
End plate	1050	820	40
Current collector	967	734.5	2
Bipolar plate	967	734.5	1
Flow frame	967	734.5	3.4
Electrode	900	500	3.4
Gasket	911	678	0.9
Membrane	967	734.5	0.125
Thick plate	967	734.5	40

3. Results and discussion

3.1. Weibull statistics for key components

The flow frame and bipolar plate are the two key components of the stack that are prone to experience damages in practice. In order to apply Weibull statistics to evaluate their failure probabilities in a stack design, the Weibull parameters (i.e. Weibull modulus m and scale parameter σ_0) for both flow frame and bipolar plate were determined by the measurements of tensile strength with 19 samples for each component. By arranging the tensile strength measurements in order, the failure probability P_i of the ith sample can be given by

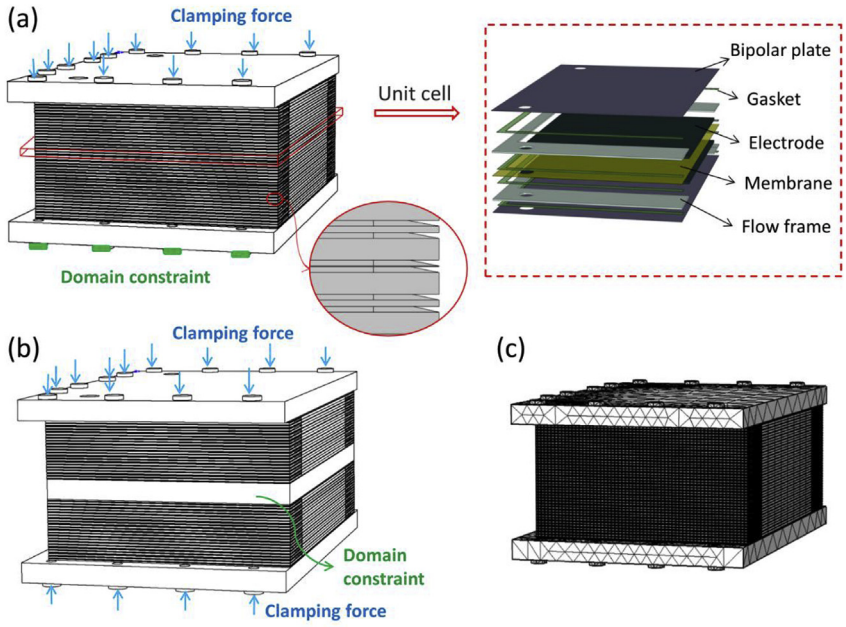

Fig. 2. Geometric models for finite element analysis. (a) 20-cell stack; (b) 20-cell-TPM stack; (c) Meshed 20-cell stack.

Table 2
Materials and properties of the stack components.

Component	Material	Young's modulus (GPa)	Poisson's ratio	Density (kg m^{-3})	Ref
End plate	Aluminum alloy	300	0.22	3900	[35]
Current collector	Copper	110	0.35	8700	[35]
Bipolar plate	Graphite Plate	3.44	0.25	1760	[36]
Flow frame	PVC	2.41	0.38	1300	[35]
Electrode	Carbon felt	0.0075	0.1	100	[37]
Gasket	EPDM	0.0078	0.47	900	[35]
Membrane	Nafion212	0.2	0.25	1968	[38]
Thick plate	PVC	2.41	0.38	1300	[35]

Table 3
Mesh independence analysis.

Element number	379,528	419,537	584,368	676,470	710,683
Stress (MPa)	30.8	32.9	36.4	40.6	41.2

$$P_i = \frac{i}{19+1} \quad (9)$$

Both the tensile strength measurements and their calculated failure probabilities are listed in Table 4. In addition, the Weibull graphs for both bipolar plate and flow frame are also plotted in Fig. 3(a) and (b) respectively. According to linear relationship between the ln (ln (1/(1-P_i))) and the ln (σ_i) shown Eq. (4), both Weibull modulus m and scale parameter σ_0 were obtained by the slope and the intercept of the linear fitting as given in Fig. 3(a) and (b). Based on the Weibull parameters and Eq. (2), the failure probabilities for the bipolar plate and flow frame as a function of stress is obtained in Fig. 3(c). A sharp increase in failure probability can be observed around the characteristics strength σ_0 for both components indicating that the failure strength ranges of the two components are relatively narrow, where the failure strength ranges are the slope ranges of the curves shown in Fig. 3(c). Namely, there is relatively clear failure strength value to assess whether the bipolar plate or the flow frame will mechanically fail.

3.2. Mechanical behaviors of the stack

In addition to the Weibull parameters, stack mechanical behaviors are also essential in evaluating the failure probability of a stack, so the finite element analysis for both stack designs described in Fig. 2 has been performed. Fig. 4 depicts the distributions of displacement for two stack designs at a clamping force of 500 kN. For the 20-cell stack design, the displacement is observed to increase from bottom to top along z-axis, which is ascribed to the applied clamping forces on the top nuts. In contrast, a minimum of displacement in the middle and increased displacements at both top and bottom sides are generated for the 20-cell-TPM stack design, primarily attributing to the clamping forces imposed from both top and bottom side in the design. It is also worth noting that

Table 4
Tensile strength measurements and failure probability.

Sample number	Failure probability, P	Flow frame	Bipolar plate
		Tensile strength (MPa), σ	
1	0.05	43.00	15.79
2	0.10	44.38	15.80
3	0.15	45.12	15.95
4	0.20	45.42	16.01
5	0.25	45.88	16.25
6	0.30	45.95	16.42
7	0.35	46.12	16.82
8	0.40	46.50	16.86
9	0.45	46.82	16.90
10	0.50	47.10	16.97
11	0.55	47.35	17.05
12	0.60	47.59	17.08
13	0.65	47.82	17.20
14	0.70	48.31	17.26
15	0.75	48.46	17.38
16	0.80	49.58	17.41
17	0.85	49.84	18.10
18	0.90	50.01	18.11
19	0.95	50.10	18.35

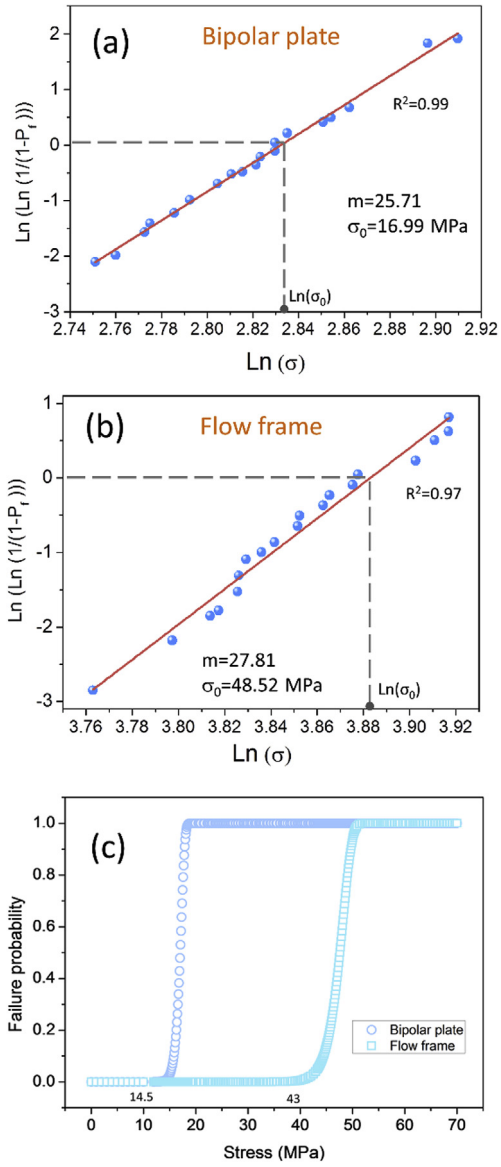

Fig. 3. Weibull graphs for (a) bipolar plate and (b) flow frame. (c) Failure probability versus stress.

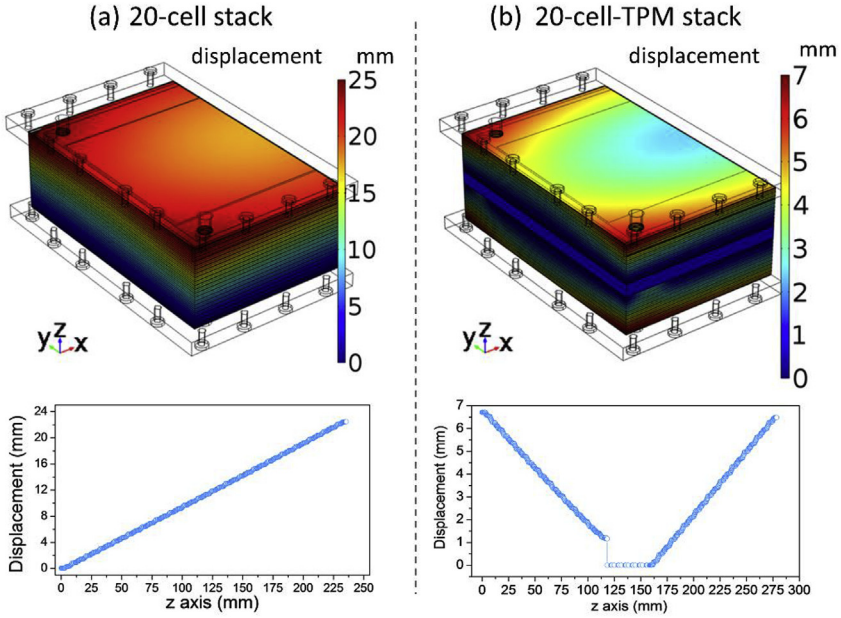

Fig. 4. Displacement distributions at a clamping force of 500 kN. (a) 20-cell stack, (b) 20-cell-TPM stack.

the maximum displacement for the 20-cell-TPM stack is much smaller than that of the 20-cell stack, indicating that the 20-cell-TPM stack design is less likely to undergo serious deformation and suffer from material failure under the same assembling forces.

To further assess the mechanical status inside the stack and perform stack failure analysis, spatial stress distributions of the flow frames and the bipolar plates are also investigated for both stack designs. First of all, maximum principal stress distributions in the 20-cell stack at a clamping force of 500 kN are shown in Fig. 5. For the bipolar plates, a maximum tensile stress of 87.2 MPa is reached around the flow inlets/outlets, which has exceeded the Weibull strength of 17.29 MPa listed in Table 5. Such a stress concentration has also been seen in fuel cell stack [37], which indicates a high risk of cracking for the bipolar plate around the flow inlets/outlets areas due to its brittle property. Apart from that, the rest of the bipolar plate receives moderate compressive stresses, e.g. the active area with a uniform stress distribution below 5 MPa. When it comes to the flow frames, the stresses are seen to mainly concentrate on the edges where the sealing gaskets are placed, with a maximum of 40 MPa below its Weibull strength of 48.23 MPa that ensures an excellent sealing performance while preventing the flow frames from plastic deformation.

Table 5
Weibull parameters.

	Flow frame	Bipolar plate
Weibull modulus, m	27.78	25.32
Weibull strength (MPa), σ_0	48.23	17.29

Secondly, maximum principal stress distributions in the 20-cell-TPM stack are also provided in Fig. 6. By placing a thick plate in the middle

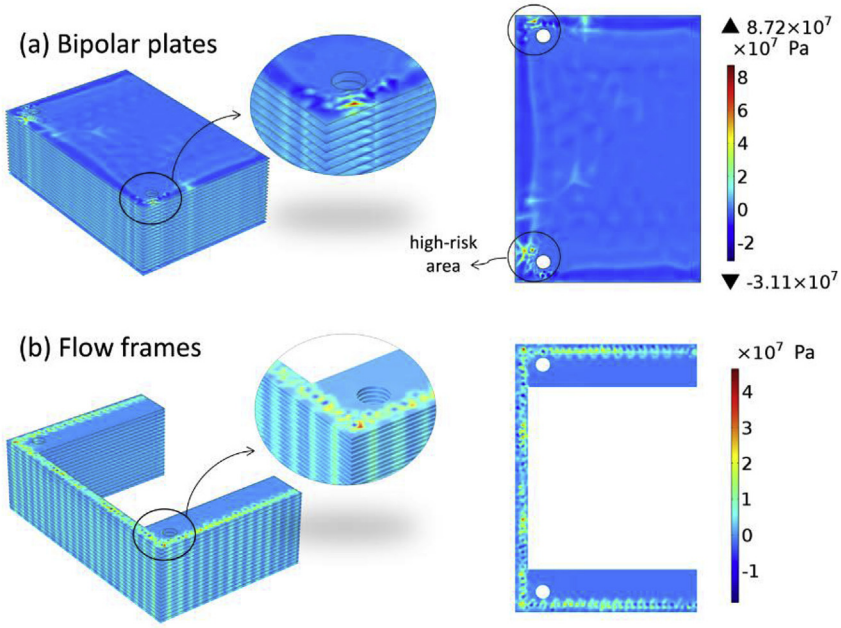

Fig. 5. Maximum principal stress distributions for the 20-cell stack at the clamping force of 500 kN. (a) Bipolar plates; (b) Flow frames.

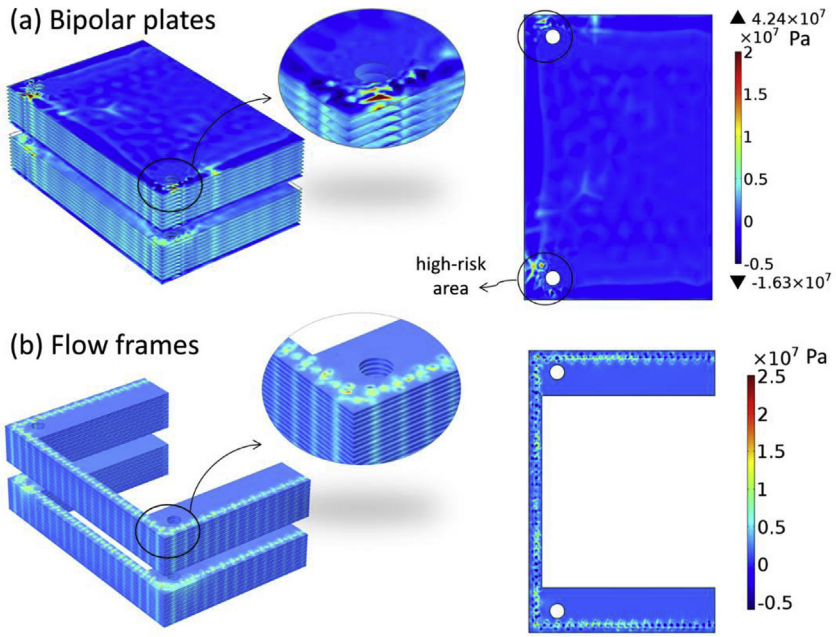

Fig. 6. Maximum principal stress distributions for the 20-cell-TPM stack at the clamping force of 500 kN. (a) Bipolar plates; (b) Flow frames.

of the stack, it can be observed that the maximum stress on inlets/outlets areas of the bipolar plates has significantly dropped from 87.2 MPa to 42.4 MPa that effectively reduces the risk of cracks, while the compressive stresses on the active area only see a slight decrease. Similar effects can be seen on the flow frames as well, where the maximum stress drops from 40 MPa to 25 MPa further reducing the risk of material damages. The above results have demonstrated that the 20-cell-TPM stack design is advantageous in reducing the maximum stress in the stack while without compromising the compressive stresses in the active area and the sealing performance of gaskets.

3.3. Failure probability of the 20-cell stack

Based on the Weibull parameters and stress analysis discussed above, failure probability of the components and the stack can be calculated according to the descriptions in Section 2. As the flow frame and bipolar plate are regarded as the most sensitive components to the material failure in practical VFB stacks, the failure probability of a VFB stack can be expressed as

$$P_{\text{stack}} = 1 - (1 - P_{\text{Bipolar plates}})\cdot(1 - P_{\text{Flow frames}}) \tag{10}$$

where $P_{\text{Bipolar plates}}$ and $P_{\text{Flow frames}}$ are the failure probabilities of the bipolar plates and the flow frames respectively. For a 20-cell stack, the $P_{\text{Bipolar plates}}$ and $P_{\text{Flow frames}}$ can be determined by

$$P_{\text{Bipolar plates}} = 1 - \prod_{i=1}^{20+1} (1 - P_{\text{Bipolar plate, } i}) \tag{11}$$

$$P_{\text{Flow frames}} = 1 - \prod_{j=1}^{2\times 20} (1 - P_{\text{Flow frame},j}) \tag{12}$$

where $P_{\text{Bipolar plate, } i}$ and $P_{\text{Flow frame, } j}$ are the failure probability of the ith bipolar plate and the jth flow frame in the stack respectively, which can be further calculated by means of the triple integration of the stress $\sigma(x, y, z)$ over the component volume V (referring to Figs. 5 and 6) as follows

$$P_{\text{Bipolar plate, } i} = 1 - \exp\left[-\iiint_{V_i} \left(\frac{\sigma(x, y, z)}{\sigma_{0,B}}\right)^{m_B} dV_i\right] \tag{13}$$

$$P_{\text{Flow frame},j} = 1 - \exp\left[-\iiint_{V_j} \left(\frac{\sigma(x, y, z)}{\sigma_{0,F}}\right)^{m_F} dV_j\right] \tag{14}$$

where m and σ_0 are the fitted Weibull parameters given in Table 5, and V_i and V_j are the volumes of the ith bipolar plate and the jth flow frame. By using Eqs. 10–14, hence, the probability of a given stack design can be readily determined by coupling Weibull statistics and finite element analysis.

Using the proposed method, the 20-cell stack design presented in Fig. 7(a) is firstly studied by applying a clamping force of 600 kN and the failure probability is analyzed in Fig. 7(b). It is observed that the all the flow frames undergo material failure with the failure probability approaching to 1 while all bipolar plates maintain good mechanical performance except for the two outer plates, revealing that the assembled stack is mechanically unreliable under a clamping force of 600 kN. By reducing the clamping force to 500 kN, it can be also seen from Fig. 7(b) that the failure probabilities of both flow frames and bipolar plates have been effectively reduced. Nevertheless, the failure probability of the 21st bipolar plate (i.e. the top plate) still remains 1, which leads to a stack failure probability of 1 and thus a mechanical failure stack. One way to reduce the failure probability of the 21st bipolar plate is to tune its mechanical property. For instance, decreasing the Young's modulus from 3.4 GPa to 1.0 GPa may reduce its failure probability to 0.21 and a subsequent stack failure probability of 0.91. However, it is difficult to fabricate such a bipolar plate with reduced Young's modulus while without compromising the conductivity and toughness. Alternatively, the clamping force can be further reduced until an acceptable stack failure probability is achieved. Fig. 7(c) reveals the variation of failure probability of the 21st bipolar plate under decreasing clamping forces. It can be observed that the failure probability of 21st bipolar plate has dropped from 1 to 0.05 with the clamping force declining from 500 kN to 400 kN, which further contributes to a dramatic decrease in stack failure probability from 0.999 to 0.03 as presented in Fig. 7(d), thus confirming an improved mechanical reliability of the stack. The results have demonstrated that the clamping force has a crucial influence in failures of the stack and its components, so an appropriate clamping force ensuring great mechanical performance needs to be carefully chosen for stack assembly in practice, while an emphasis should also be given on the materials of components and their mechanical properties.

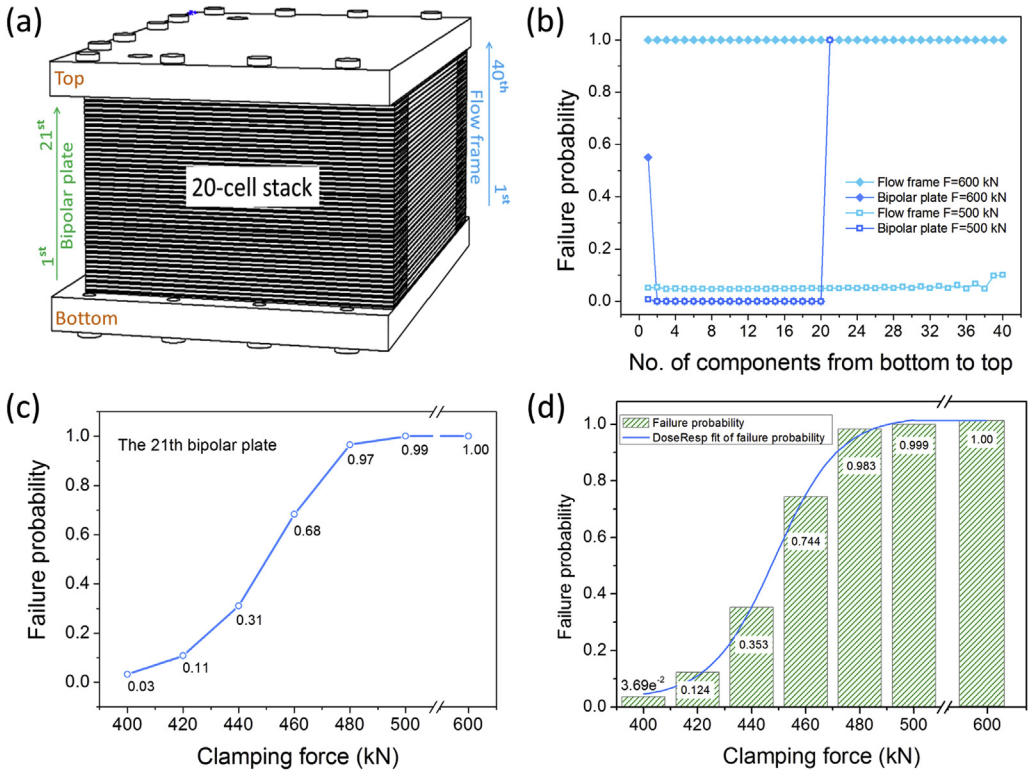

Fig. 7. Failure probability analysis for the 20-cell stack design. (a) Stack design illustration; (b) Failure probabilities of bipolar plates and flow frames; (c) Failure probability of the 21st bipolar plate under varying clamping forces; (d) Stack failure probability as a function of clamping force.

3.4. Failure probability of the 20-cell-TPM stack

To evaluate the effects of assembling condition and design on mechanical performance of the VFB stack, the 20-cell-TPM stack is subsequently studied as a comparison. An illustration of the design can be referred to Fig. 8(a), where is shown that an additional bipolar plate is required for this specific design. Thus, the failure probability of bipolar plates with a total number of 22 can be expressed as

$$P_{\text{Bipolar plates}} = 1 - \prod_{i=1}^{22} \exp\left[-\iiint_{V_i} \left(\frac{\sigma(x, y, z)}{17.29} \right)^{25.32} dV_i \right] \quad (15)$$

As a comparison, a clamping force of 600 kN is initially applied to the 20-cell-TPM stack design and the failure probabilities of bipolar plates and flow frames are given in Fig. 8(b). It can be observed that both bipolar plates and flow frames have a very low probability of failure under 600 kN while the stack further demonstrates a failure probability of c.a. 0.01% in contrast to a failure probability of 1 for the 20-cell stack design. Such an improvement in prevention of failure is beneficial from the use of an additional thick plate placing in the middle of the stack which strongly enhances the mechanical stability and robustness of the stack. The results also indicate that an increase in clamping forces over 600 kN imposed on the 20-cell-TPM stack is possible as the stack failure probability shows to be only 0.01%. Fig. 8(c) provides the stack failure probability as a function of increased clamping forces, in which it is seen that the stack failure probability starts with a tiny increase from 600 kN to 700 kN, followed by a sharp increase at 750 kN and finally a reach of 1 at 900 kN. Compared with the results of the 20-cell stack in Fig. 7(d) where a clamping force of 440 kN yields a stack failure probability of 0.353, the 20-cell-TPM stack can achieve a same level of stack failure probability of 0.37 with a much larger clamping force of 800 kN. Such an increase in clamping force without compromising the failure probability is highly favorable in stack design and assembly for achieving a better sealing performance and a significant reduction in contact resistance of the stack. By comparing the failure probabilities for the two investigated stack designs under specified assembling conditions, therefore, it can be concluded that the 20-cell-TPM stack design is generally superior to the 20-cell stack design in terms of both mechanical performance and battery efficiency. Besides, it also demonstrates the feasibility of the proposed Weibull statistics based failure analysis, so flow battery engineers should be able to readily access the approach in design and assembly of commercial VFB stacks.

4. Conclusions

In this study, mechanical behavior and Weibull statistics based failure analysis of the stacks have been carried out for the all-vanadium redox flow battery. Two key stack components, i.e. bipolar plate and flow frame, were firstly fabricated and their Weibull parameters were determined from the tensile strength tests. Subsequently, the mechanical behavior and failure probability of two different stack designs both containing 20 individual cells were evaluated by finite element analysis and Weibull statistics method. The results demonstrated that the stack failure probability is closely associated with the materials, the stack design and assembling forces. In the 20-cell stack design, the composite bipolar plates play a crucial role in determining the stack failure, where the stack failure probability would drop from 1 to 0.03 with the clamping force decreasing from 500 kN to 400 kN. In contrast, the 20-cell-TPM stack sees a dramatic decrease in failure probabilities of both key components and the stack under the same clamping forces ascribed to the improved mechanical stability by placing an additional thick plate in the middle of the stack, thus proving superior mechanical and sealing performance as well as a positive impact in reduction of the contact resistance of the stack. Such a stack failure analysis approach proposed in this study is particularly useful for design and assembly of commercial VFB stacks and can be readily accessed by flow battery engineers. Besides, the failure analysis of the stack materials along with the Weibull statistics can also help to select premium materials,

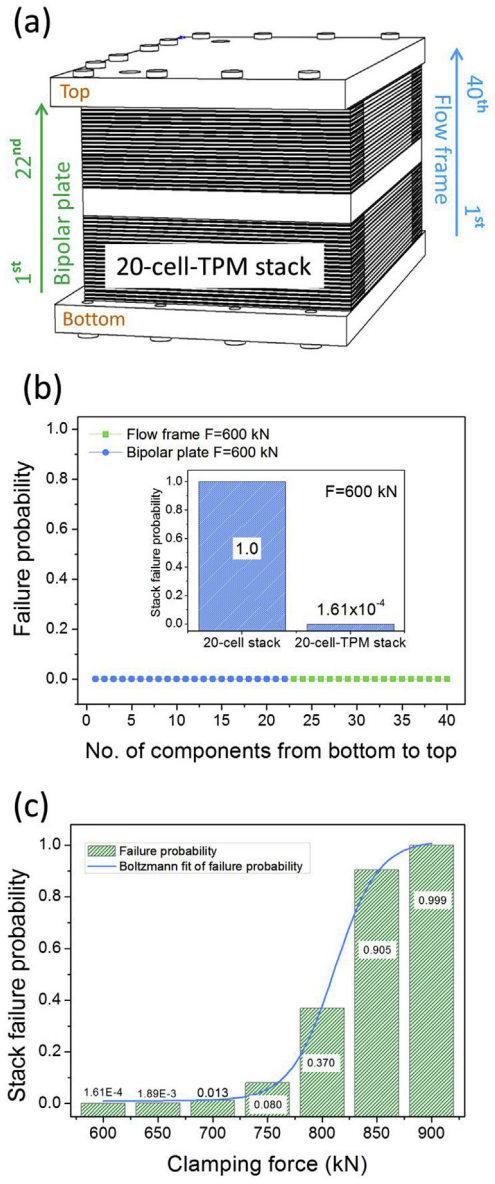

Fig. 8. Failure probability analysis for the 20-cell-TPM stack design. (a) Stack design illustration; (b) Failure probabilities at 600 kN; (c) Stack failure probability as a function of clamping force.

optimize the compositions and improve the fabrication processes. To ensure a long-term stack mechanical and sealing performance in reality, however, mechanical properties of other components of the stack (e.g. sealing gasket) and operating conditions (e.g. flowing and thermal conditions) also need to be considered and included in future studies.

Acknowledgments

This work is supported by the National Nature Science Foundation of China (Grant No. 21706266) and Institute of Metal Research, Chinese Academy of Sciences. We also thank Shaoyu Hou and Hai Gao for the technical support.

Appendix A. Supplementary data

Supplementary data to this article can be found online at https://doi.org/10.1016/j.jpowsour.2018.11.060.

References

[1] P. Leung, A.A. Shah, L. Sanz, C. Flow, J.R. Morante, Q. Xu, M.R. Mohamed, C. Ponce de Leon, F.C. Walsh, Recent developments in organic redox flow batteries: a critical review, J. Power Sources 360 (2017) 243–283.
[2] M. Skyllas-Kazacos, M.H. Chakrabarti, A. Hajimolana, F.S. Mjalli, M. Saleem, Progress in flow battery research and development, J. Electrochem. Soc. 158 (2011) R55–R79.
[3] M. Skyllas-Kazacos, G. Kazacos, G. Poon, H. Verseema, Recent advances with UNSW vanadium-based redox flow batteries, Int. J. Energy Res. 34 (2010) 182–189.
[4] C. Minke, U. Kunz, T. Turek, Techno-economic assessment of novel vanadium redox flow batteries with large-area cells, J. Power Sources 361 (2017) 105–114.
[5] Y. Yan, Y. Li, M. Skyllas-Kazacos, J. Bao, Modelling and simulation of thermal behavior of vanadium redox flow battery, J. Power Sources 322 (2016) 116–128.
[6] M. Al-Yasiria, J. Park, A novel cell design of vanadium redox flow batteries for enhancing energy and power performance, Appl. Energy 222 (2018) 530–539.
[7] Q. Wang, Z.G. Qu, Z.Y. Jiang, W.W. Yang, Experimental study on the performance of a vanadium redox flow battery with non-uniformly compressed carbon felt electrode, Appl. Energy 213 (2018) 293–305.
[8] D. Park, K.S. Jeon, C.H. Ryu, G.J. Hwang, Performance of the all-vanadium redox flow battery stack, J. Ind. Eng. Chem. 45 (2017) 387–390.
[9] C. Minke, T. Turek, Economics of vanadium redox flow battery membranes, J. Power Sources 286 (2015) 247–257.
[10] B. Jiang, L. Wu, L. Yu, X. Qiu, J. Xi, A comparative study of Nafion series membranes for vanadium redox flow batteries, J. Membr. Sci. 510 (2016) 18–26.
[11] Y.K. Zeng, X.L. Zhou, L. An, L. Wei, T.S. Zhao, A high-performance flow-field structured iron-chromium redox flow battery, J. Power Sources 324 (2016) 738–744.
[12] X. Kea, J.M. Prahla, J. Iwan, D. Alexander, Robert F. Savinell, Redox flow batteries with serpentine flow fields: distributions of electrolyte flow reactant penetration into the porous carbon electrodes and effects on performance, J. Power Sources 384 (2018) 295–302.
[13] B. Caglar, P. Fischer, P. Kauranen, M. Karttunen, P. Elsner, Development of carbon nanotube and graphite filled polyphenylene sulfide based bipolar plates for all-vanadium redox flow batteries, J. Power Sources 256 (2014) 88–95.
[14] J. Choe, J.W. Lim, M. Kim, J. Kim, D.G. Lee, Durability of graphite coated carbon composite bipolar plates for vanadium redox flow batteries, Compos. Struct. 134 (2015) 106–113.
[15] X.L. Zhou, Y.K. Zeng, X.B. Zhu, L. Wei, T.S. Zhao, A high-performance dual-scale porous electrode for vanadium redox flow batteries, J. Power Sources 325 (2016) 329–336.
[16] T. Liu, X. Li, H. Zhang, J. Chen, Progress on the electrode materials towards vanadium flow batteries (VFBs) with improved power density, J. Energy Chem. 27 (2018) 1292–1303.
[17] P. Liang, D. Qiu, L. Peng, P. Yi, X. Lai, J. Ni, Structure failure of the sealing in the assembly process for proton exchange membrane fuel cells, Int. J. Hydrogen Energy 42 (2017) I0217–I0227.
[18] D. Ye, Z. Zhan, A review on the sealing structures of membrane electrode assembly of proton exchange membrane fuel cells, J. Power Sources 231 (2013) 285–292.
[19] J. Xiong, M. Jing, A. Tang, X. Fan, J. Liu, C. Yan, Mechanical modelling and simulation analyses of stress distribution and material failure for vanadium redox flow battery, J. Energy Storage 15 (2018) 133–144.
[20] Y. Luo, W. Jiang, Q. Zhang, W.Y. Zhang, M. Hao, Effects of anode porosity on thermal stress and failure probability of planar solid oxide fuel cell with bonded compliant seal, J. Hydrogen Energy 41 (2016) 7464–7474.
[21] A. Nakajo, Z. Wuillemin, J.V. herle, D. Favrat, Simulation of thermal stresses in anode-supported solid oxide fuel stacks. Part I: probability of failure of the cells, J. Power Sources 193 (2009) 203–215.
[22] G. Anandakumar, N. Li, A. Verma, P. Singh, J. Kim, Thermal stress and probability of failure analyses of functionally graded solid oxide fuel cells, J. Power Sources 195 (2010) 6659–6670.
[23] Y. Wang, W. Jiang, Y. Luo, Y. Zhang, S. Tu, Evolution of thermal stress and failure probability during reduction and re-oxidation of solid oxide fuel cell, J. Power Sources 371 (2017) 65–76.
[24] R. Clague, A.J. Marquis, N.P. Brandon, Time independent and time dependent probability of failure of solid oxide fuel cells by stress analysis and the Weibull method, J. Power Sources 221 (2013) 290–299.
[25] F. Greco, H.L. Frandsen, A. Nakajo, M.F. Madsen, J.V. herle, Modelling the impact of creep on the probability of failure of a solid oxide fuel stack, J. Eur. Ceram. Soc. 34 (2014) 2695–2704.
[26] W. Weibull, A statistical distribution function of wide applicability, J. Appl. Mech. 18 (1951) 293–297.
[27] A. De S. Jayatilaka, Fracture of Engineering Brittle Materials, Applied Science Publishers, London, 1979.
[28] D. Zhang, M. Abendroth, M. Kuna, J. Storm, Multi-axial brittle failure criterion using Weibull stress for open Kelvin cell foams, Int. J. Solid Struct. 75 (2015) 1–11.
[29] T. Zhang, Q. Zhu, W.L. Huang, Z. Xie, X. Xin, Stress field and failure probability analysis for the single cell of planar solid oxide fuel cells, J. Power Sources 182 (2008) 540–545.
[30] A. Salem, R. Akbari Sene, Optimization of zeolite-based adsorbent composition for fabricating reliable Raschig ring shaped by extrusion using Weibull statistical theory, Microporous Mesoporous Mater. 163 (2012) 65–75.
[31] G. Quercia, D. Chan, K. Luke, Weibull statistics applied to tensile testing for oil well cement compositions, J. Petrol. Sci. Eng. 146 (2016) 536–544.
[32] L.F. Liu, B. Liu, C.W. Wu, Reliability prediction of large fuel stack based on structure

stress analysis, J. Power Sources 363 (2017) 95–102.
[33] W. Weibull, Statistical theory of strength of materials (151), Ingeniors Vetenskaps Akademien, Handlingar, vol. 45, 1939.
[34] I. Gatto, F. Urbani, G. Giacoppo, Influence of the bolt torque on PEFC performance with different gasket materials, Int. J. Hydrogen Energy 36 (2011) 13043–13050.
[35] W.D. Callister, D.G. Rethwisch, Material Science and Engineering: an Introduction, ninth ed., Wiley, America, 2014.
[36] Entegris, Cell Stack Plates: Typical Material Properties, BCM 8649. http://www.entegris.com/Resources/assets/6002-2153-0312.pdf (accessed March 2017).
[37] J. Cruz, U. Cano, T. Romero, Simulation and in situ measurement of stress distribution in a polymer electrolyte membrane fuel cell stack, J. Power Sources 329 (2016) 273–280.
[38] DuPont Fuel Cells, NR211 and NR212: Properties of Nagion® PFSA Membrane. http://fuelcellstore.com/spec-sheets/nafion-211-212-spec-sheet.pdf.